Exsolution of SrO during the topochemical conversion of $LaSr_3CoRuO_8$ to the Oxyhydride $LaSr_3CoRuO_4H_4$

Exsolution of SrO during the topochemical conversion of $LaSr_3CoRuO_8$ to the oxyhydride $LaSr_3CoRuO_4H_4$

Lun Jin[†], Maria Batuk[‡], Franziska K. K. Kirschner[⊗], Franz Lang[⊗], Stephen J. Blundell[⊗], Joke Hadermann[‡] and Michael A. Hayward[†]*

† Department of Chemistry, University of Oxford, Inorganic Chemistry Laboratory, South Parks Road, Oxford, OX1 3QR, U.K.

‡EMAT, University of Antwerp, Groenenborgerlaan 171, B-2020 Antwerp, Belgium.

⊗Department of Physics, Clarendon Laboratory, University of Oxford, Parks Road, Oxford, OX1 3PU, UK.

ABSTRACT: Reaction of the $n = 1$ Ruddlesden-Popper oxide $LaSr_3CoRuO_8$ with CaH_2 yields the oxyhydride phase $LaSr_3CoRuO_4H_4$ via topochemical anion-exchange. Close inspection of X-ray and neutron powder diffraction data in combination with HAADF-STEM images reveals that nanoparticles of SrO are exsolved from the system during the reaction, with the change in cation stoichiometry accommodated by the inclusion of $n > 1$ $(Co/Ru)_nO_{n+1}H_{2n}$ 'perovskite' layers into the Ruddlesden-Popper stacking sequence. This novel pseudo-topochemical process offers a new route for the formation of $n > 1$ Ruddlesden-Popper structured materials. Magnetization data are consistent with a $LaSr_3Co^{1+}Ru^{2+}O_4H_4$ (Co^{1+}, d^8, $S = 1$; Ru^{2+}, d^6, $S = 0$) oxidation/spin state combination. Neutron diffraction and μ^+SR data show no evidence for long-range magnetic order down to 2 K, suggesting the diamagnetic Ru^{2+} centers impede the Co-Co magnetic exchange interactions.

Structure-conserving topochemical reactions allow the preparation of metastable solid-state compounds which cannot be easily synthesized by conventional high-temperature ceramic routes. By utilizing the differences in rates of diffusion, which correspond to differences in reactivity in the solid state, the most mobile species (cations, anions and molecules) can be inserted or removed from a host lattice, or exchanged for other mobile species, to yield new extended solid-state compounds.

This synthetic approach has been widely applied to complex transition metal oxides.[1-3] For example, in systems where metal cations are the most mobile species, the reductive insertion of group I metals, particularly lithium, has been used widely to prepare phases with transition metal cations in unusually low oxidation states,[4] such as the Mo^{3+} phase $LiMoO_2$ or the Ru^{3+} phase $Li_{0.9}RuO_2$,[5-6] prepared by lithium insertion into the corresponding MO_2 rutile oxide. The reverse reaction, oxidative cation extraction, has been used to prepare metastable forms of TiO_2, such as $TiO_2(R)$ and $TiO_2(H)$,[7-9] but is much more widely employed as part of the reversible lithium extraction/insertion process which is the key operating step in the charge and discharge of lithium ion battery cathode materials.[10-11] A wide range of topochemical cation exchange reactions have also been reported for complex transition metal oxides because monovalent and divalent cations can have high mobility in oxide frameworks at modest temperatures, so isovalent cation exchange reactions, such as the formation of $NaLaNb_2O_7$ from $RbLaNb_2O_7$,[12-13] or aliovalent cation exchanges, such as the formation of $Ca_{x/2}CoO_2$ from Na_xCoO_2,[14-15] are possible in a large number of systems, enabling a large range of metastable phases to be prepared.

There are an equivalent set of topochemical reactions in which anions are the most mobile species. Reductive topochemical extraction of oxide ions has been used widely, particularly in transition-metal systems with the perovskite structure, to prepare phases containing such unusual metal oxidation states as Mn^{1+}, Ni^{1+}, Ru^{2+} and Ir^{2+} [16-22] and also systems in which the transition-metal cation resides in an usual coordination geometry, such as square-planar Fe^{2+}.[23-25] Oxidative anion insertion can similarly be used to prepare phases with elevated transition metal oxidation states, such as the Ru^{5+} centers in $Sr_3Ru_2O_7F_2$, which is prepared via the topochemical fluorine insertion of $Sr_3Ru_2O_7$.[26] In addition, anion insertion can also be used to induce or modify the structural distortions of the host framework, for example breaking the inversion symmetry of a phase,[27] and in combination, the reversible topochemical insertion/extraction of anions finds application in oxygen storage materials which are used to enhance the efficiency of combustion processes.[28] Topochemical anion-exchange reactions in which oxide ions from the host material are replaced by fluoride, hydride or nitride hetro-anions have also been demonstrated and utilized to make a range of mixed anion solids.[29-30] For example, binary metal hydrides, such as CaH_2 have been shown to affect reductive hydride-for-oxide anion-exchange reactions such as the conversion of $LaSrCoO_4$ to $LaSrCoO_3H_{0.7}$ [31] or the conversion of $SrVO_3$ to $SrVO_2H$,[32] where the resulting oxyhydride phases are metastable and not preparable by more direct synthesis routes.

As a compliment to simple topochemical insertion, extraction and exchange reactions there is a class of reaction which can be considered as pseudo-topochemical, because some of the structural features of the host are retained, but the overall topology

of the structure is changed. For example, dehydration of the layered phase $HTiNbO_5$ yields $Ti_2Nb_2O_9$ in which the separated layers of the initial phase have been 'welded' together in the product via new metal-oxygen links.[33-34] Similar reactions are observed for protonated Ruddlesden-Popper phases. For example, dehydration of $H_2La_2Ti_3O_{10}$ yields the A-site cation deficient perovskite $La_2Ta_3O_9$.[12] Thus it can be seen that by utilizing and combining these different topochemical processes a wide range of complex solid compounds can be prepared which are synthetically inaccessible via conventional high temperature routes.

Recently we have been investigating the anion-based topochemical reactions of 3d/4d transition metal oxides.[16-17, 35-36] Here we report the conversion of the $n = 1$ Ruddlesden-Popper oxide $LaSr_3CoRuO_8$ to the oxyhydride $LaSr_3CoRuO_4H_4$. However, unlike the analogous conversion of $LaSr_3NiRuO_8$ to $LaSr_3NiRuO_4H_4$,[36] which is a simple, purely topochemical anion-exchange process, the formation of $LaSr_3CoRuO_4H_4$ occurs with exsolution of SrO and the inclusion of $n > 1$ defect layers. We believe this exsolution process represents the first example in a new class of a pseudo-topochemical reactions.

Results and Discussion

Structural characterization of $LaSr_3CoRuO_8$. NPD data (D2b, ILL) collected from $LaSr_3CoRuO_8$ at room temperature could be readily indexed using a body-centered tetragonal unit cell ($a = 3.874$ Å, $c = 12.625$ Å) consistent with a cation-disordered $n = 1$ Ruddlesden-Popper structure. Thus, a model based on the structure of $LaSr_3NiRuO_8$ but with Ni replaced by Co, was refined against the data.[36] All atomic positional and displacement parameters were refined freely, and the refinement converged to give a good statistical fit ($\chi^2 = 4.13$) as shown in Figure S1, and described in Tables S1 and S2 in the Supporting Information. To confirm the absence of a structural distortion or any microstructural features, high-resolution SXRD data (I11, DLS) were collected from $LaSr_3CoRuO_8$. The $n = 1$ Ruddlesden-Popper model which was refined against the neutron diffraction data was also refined against the SXRD data and also achieved a good fit ($\chi^2 = 6.38$), with no indication of a structural distortion or microstructural features, as shown in Figure S2 in the Supporting Information.

Reactivity of $LaSr_3CoRuO_8$ with CaH_2. Mixtures of $LaSr_3CoRuO_8$ and CaH_2 (Sample A) were heated sequentially for 7 day periods at temperatures between 350 and 460 ℃. Heating at temperatures up to 375 ℃ led to no reaction as observed by powder XRD data. In the temperature range $375 < T/℃ < 425$ an orthorhombic phase ($a = 3.80$ Å, $b = 3.61$ Å, $c = 13.17$ Å) formed, which was identified as $LaSr_3CoRuO_6$ and will be described in detail elsewhere. On raising the temperature to 450 ℃ a tetragonal phase formed ($a = 3.64$ Å, $c = 13.35$ Å). However, in order to achieve complete conversion of the sample to this final tetragonal phase a reaction temperature of 460 ℃ was required. Samples B and C of '$LaSr_3CoRuO_4H_4$' were prepared by heating $LaSr_3CoRuO_8/CaH_2$ mixtures directly at 450/460 ℃ as described above.

Structural characterization of '$LaSr_3CoRuO_4H_4$'. Neutron powder diffraction data (WISH, ISIS) collected at room temperature from sample B could be indexed using a body-centered tetragonal unit cell ($a = 3.64$ Å, $c = 13.35$ Å) suggesting a $LaSr_3CoRuO_4H_4$ oxyhydride phase, analogous to

$LaSr_3NiRuO_4H_4$ had formed, as shown in Figure 1. Thermogravimetric data collected during the reoxidation of the material back to $LaSr_3CoRuO_8$ indicated a mass gain of 9.32%,
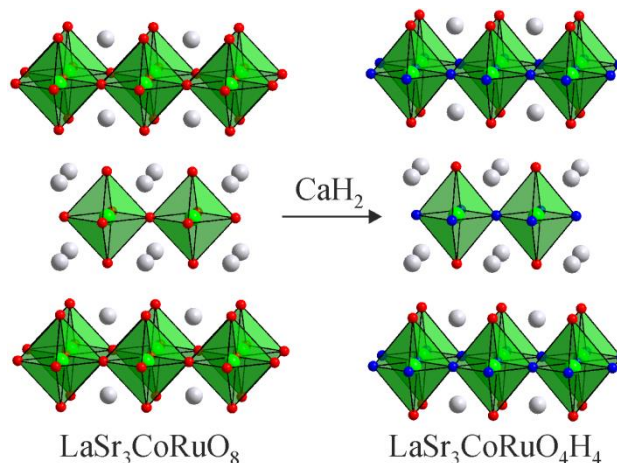

Figure 1. Crystal structures of $LaSr_3CoRuO_8$ and $LaSr_3CoRuO_4H_4$. Grey, green, red and blue sphere represent La/Sr, Co/Ru, O and H respectively.
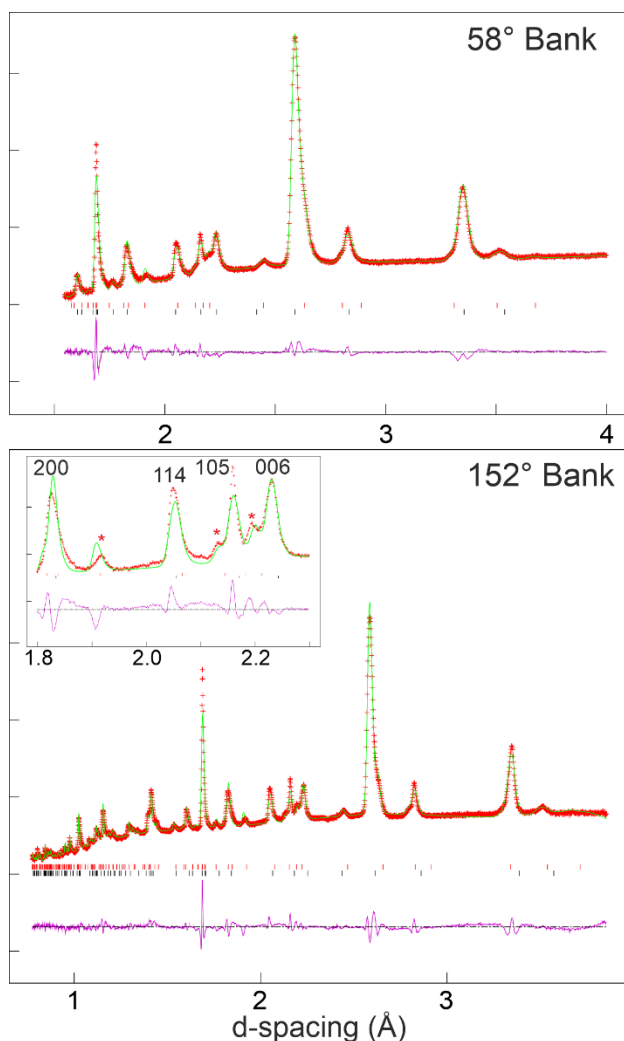

Figure 2. Observed calculated and difference plots from the refinement of a 2-phase model against NPD diffraction data collected from sample B of $LaSr_3CoRuO_4H_4$. Inset to lower panel shows poor

fitting of reflections from majority phase. Peaks from minority phase are marked with red stars in inset.

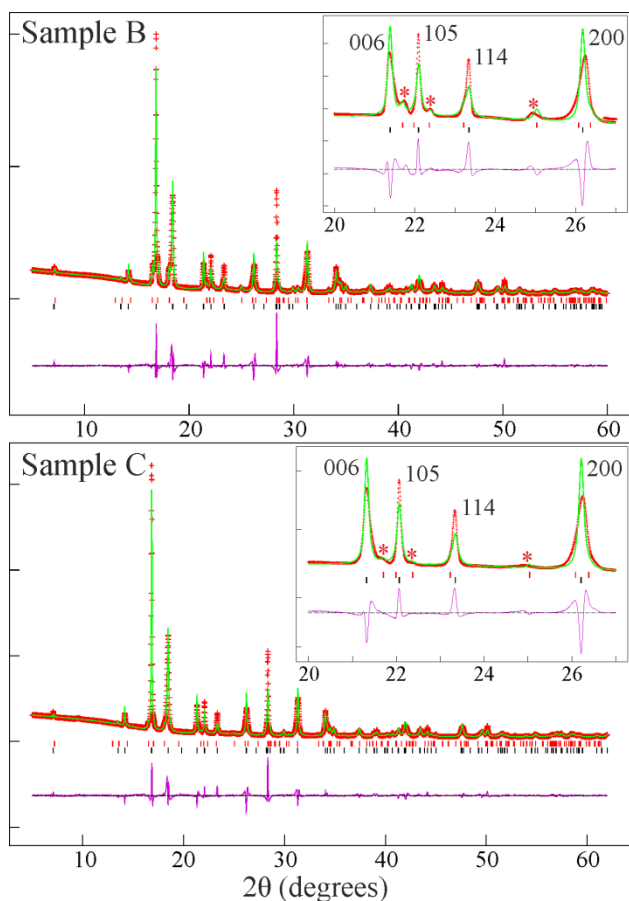**Figure 3.** Observed calculated and difference plots from the refinement of 2-phase models against SXRD data collected from samples B and C of $LaSr_3CoRuO_4H_4$. Insets show poor fitting of reflections from majority phase. Peaks from minority phase are marked with red stars in insets.

consistent with this composition. A structural model based on $LaSr_3NiRuO_4H_4$ but with nickel replaced by cobalt, was refined against the data. Close inspection revealed a series of weak diffraction reflections not accounted for by the $LaSr_3CoRuO_4H_4$ structural model which could be indexed using a body-centered orthorhombic unit cell ($a = 3.80$ Å, $b = 3.61$ Å, $c = 13.17$ Å) consistent with the intermediate phase observed during the reaction of $LaSr_3CoRuO_8$ and CaH_2 described above. Thus a 2-phase model ($LaSr_3CoRuO_4H_4$ + $LaSr_3CoRuO_6$) was refined against the data, which converged rapidly to give stable structural models for the 2 phases, detailed in Table S3 in the Supporting Information. Close inspection of the fits to the data (Figure 2, and Figure S3 in the Supporting Information) revealed that while the lower resolution data collected using the 58° detector bank were fitted acceptably, higher resolution data collected using the 152 ° detector bank were fitted poorly by the structural model, as highlighted in the inset to Figure 2. To further investigate these features of the NPD data, high-resolution SXRD data (I11, DLS) were collected from sample B of '$LaSr_3CoRuO_4H_4$'. A 2-phase $LaSr_3CoRuO_4H_4$ + $LaSr_3CoRuO_6$ model was refined against the SXRD data and, as shown in Figure 3, again there are significant peak shape mismatches between the model and observed data. To ensure that the complex

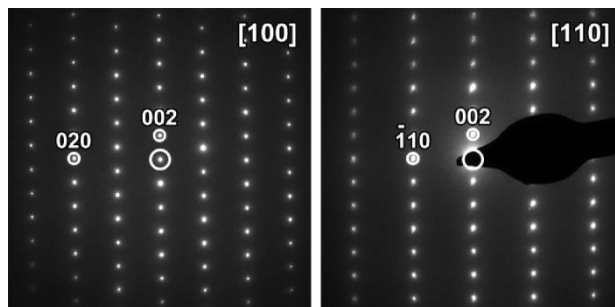peak shapes observed in the SXRD data from sample B were not due to the incomplete conversion of $LaSr_3CoRuO_6$ into $LaSr_3CoRuO_4H_4$,

Figure 4. ED patterns of sample C of $LaSr_3CoRuO_4H_4$ taken along the [100] and [110] directions.

analogous SXRD data were collected from sample C, which contains only very small amounts of $LaSr_3CoRuO_6$. However, as can be seen in Figure 3, the asymmetric diffraction peak profiles persist in the data from sample C, indicating this is an intrinsic feature of '$LaSr_3CoRuO_4H_4$'.

To investigate a possible structural distortion of '$LaSr_3CoRuO_4H_4$' from the $I4/mmm$ model refined for the phase, ED patterns were collected from several crystallites of sample C oriented along [100] and [101] directions. As shown in Figure 4, the ED patterns can be indexed using $I4/mmm$ symmetry with lattice parameters $a \approx 3.6$ Å, $c \approx 13.3$ Å, with no sign of superstructure reflections, consistent with the model refined against the neutron and synchrotron X-ray diffraction data. The lack of any evidence for a symmetry lowering structural distortion suggests that the poor fit to the bulk diffraction data is due to the local microstructure of the sample.

Microstructural characterization of '$LaSr_3CoRuO_4H_4$'. HAADF-STEM images collected from sample C of '$LaSr_3CoRuO_4H_4$' indicate that many, but not all, crystallites of the sample are covered in crystalline nanoparticles (as shown in Figure S4, in the Supporting Information). Given that the sample was not exposed to air, and that the nanoparticles were seen from the beginning of the imaging experiment so are not due to beam induced damage, we deduce that they are an intrinsic part of the sample and, as we will show later, are SrO particles exsolved from the Co/Ru phases during the anion exchange process.

Figure 5(a) shows a HAADF-STEM image of a highly crystalline particle aligned along the [100] direction. The bright spots in the image indicate columns of high Z atoms, which can be recognized as columns of La/Sr and Co/Ru cations, and thus the image in Figure 5(a) is consistent with a region with the tetragonal, $n = 1$ structure proposed for $LaSr_3CoRuO_4H_4$. However, other HAADF-STEM images collected from sample C, shown in Figures 5(b) and (c) indicate that in other particles the regular $n = 1$ Ruddlesden-Popper stacking is interrupted by intergrowths of $n = 2$ and $n = 4$ stacking. Intensity profiles measured across these images as indicated in Figure 5(b) and (c), reveal that the A-cation layers in the centers of these intergrowth blocks – especially noticeable in the $n = 2$ intergrowths in Figure 5(b) – tend to have a higher intensity than the bulk $n = 1$ regions. This intensity enhancement is consistent with a higher average Z for the cations in these positions, suggesting it is likely they are lanthanum rich, compared to the values expected for $LaSr_3CoRuO_4H_4$.

To confirm that the intergrowths observed in the HAADF-STEM images are responsible for the asymmetric peak profiles observed in the bulk diffraction data, an analysis using
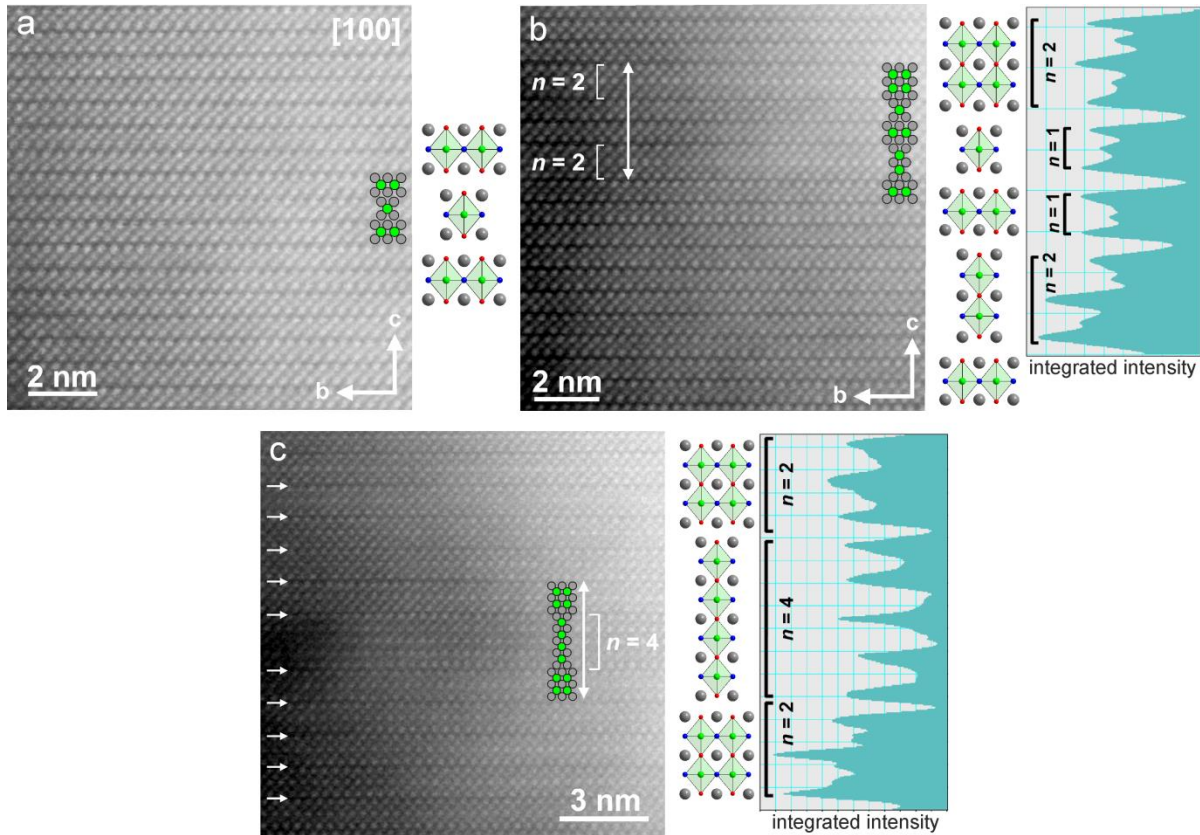

Figure 5. HAADF-STEM images of aligned crystallites of Sample C. Image (a) shows a crystalline region without planar defects. Image (b) shows an array of $n = 1$ layers with $n = 2$ defects and image (c) shows $n = 2$ array with an $n = 4$ defect layer. Horizontal arrows in (c) highlight rock-salt layer positions. Intensity profiles measured along the vertical arrows are shown to the right of each image (the signal is averaged along the b axis) and indicate the A-cation layers in the middle of the perovskite blocks of the $n = 2$ fragments are brighter than at the periphery and that they are therefore most likely La-rich.

the FAULTS software package was performed.[37] Diffraction patterns were calculated, as described in detail in the supporting information, for two different scenarios.

In the first scenario the planar defects were modelled as isolated intergrowths of $n = 2$ $LaSr_2CoRuO_3H_4$ blocks within a matrix of 'perfect' $LaSr_3CoRuO_4H_4$ layers. Figure 6 shows how the calculated synchrotron X-ray diffraction patterns evolve with increasing defect-layer concentration, compared to the measured data from sample C, and it can be seen that the [105] reflection rapidly becomes broader and weaker than observed. In addition the calculated profiles of the [006] and [114] reflections do not exhibit the marked asymmetry which can be seen in the observed data, indicating this 'isolated defect' scenario is a poor description of the planar defects in the system.

In a second scenario $n = 2$ defects layers were allowed to aggregate in the model. Thus, compared to scenario 1 where the probability of having two adjacent $n = 2$ planar defects is zero, in this second scenario this probability was allowed to take non-zero values. Figure 7 shows a series of calculated diffraction profiles in which the concentration of $n = 2$ defect layers was kept constant at 14%, but the frequency of adjacent defects was increased systematically, as described in detail in the Supporting Information. As the defect layers aggregate, it can be seen that the [105] peak sharpens and the [006] and [114] reflections

become asymmetric, as observed in the experimental data, suggesting this second scenario is a
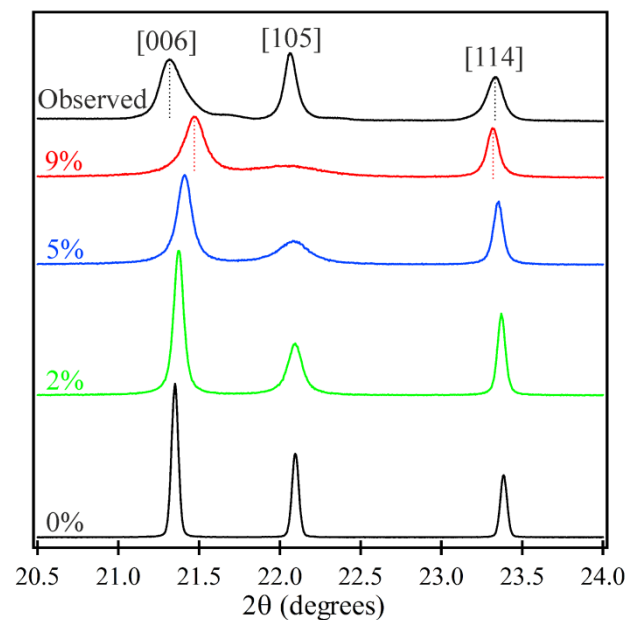
Figure 6. Calculated SXRD profiles for structural models containing increasing concentrations of isolated $n = 2$, $LaSr_2CoRuO_3H_4$ defect layers within a matrix of perfect n = 1, $LaSr_3CoRuO_4H_4$ layers. The experimental SXRD data collected from sample C of '$LaSr_3CoRuO_4H_4$' is also plotted for comparison.
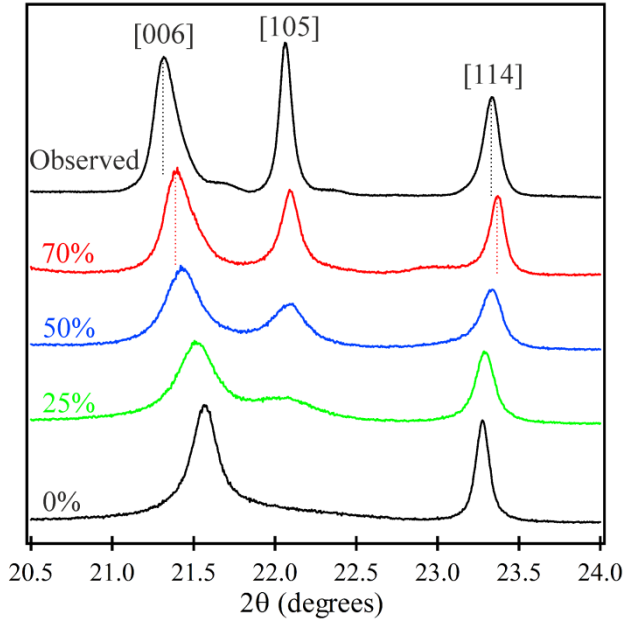

Figure 7. Calculated SXRD profiles for structural models containing a 14% concentration of $n = 2$ defect layers in which the degree of defect aggregation (probability of adjacent defect layers) is allowed to increase. The experimental SXRD data collected from sample C of '$LaSr_3CoRuO_4H_4$' is also plotted for comparison.

better description of the planar defects in the system. This is consistent with the extended region of n = 2 stacking seen in Figure 5(c). The inclusion of $n = 3$ or $n = 4$ defect layers within the model, did not change the simulated diffraction profiles noticeably. It was not possible to quantify the concentration of defect layers by fitting the diffraction data, because all patterns exhibit a small, hkl dependent peak broadening ($hk0$ broader than $00l$, in common with $LaSr_3NiRuO_4H_4$ and $(La/Sr)_2M_{0.5}Rh_{0.5}O_3H$ oxyhydride phases) [35-36] which cannot be modelled within the FAULTS code.[37]

The observations described above suggest a mechanism for the formulation of the $n > 1$ intergrowths observed within '$LaSr_3CoRuO_4H_4$' in which $LaSr_3CoRuO_8$ is initially converted to $LaSr_3CoRuO_6$ via anion deintercalation. This anion-deficient phase is then converted to $LaSr_3CoRuO_4H_4$ via a redox-neutral anion-exchange, but once formed $LaSr_3CoRuO_4H_4$ exsolves SrO, again in a redox-neutral process, to first make layers of the $n = 2$ phase $LaSr_2CoRuO_3H_4$ and then further SrO is exsolved to make blocks of $La_{n/2}Sr_{1+n/2}Co_{n/2}Ru_{n/2}O_{n+1}H_{2n}$ with $n > 2$. This reaction pathway is consistent with the observations made during reactions, and with those made of the washed product phases, and as noted above suggests that the nanoparticles observed on the surface of crystallites are the SrO exsolved during the formation of the intergrowth layers.

The accumulation and aggregation of $n > 1$ defect layers during the conversion of $LaSr_3CoRuO_8$ to '$LaSr_3CoRuO_4H_4$' suggests, at least in principle, that if this process continued the $n = \infty$ phase, $LaSrCoRuO_2H_4$ could be formed. To investigate this possibility by furthering the exsolution of SrO, and increasing

the number of $n > 1$ defective layers, aliquots of sample C of '$LaSr_3CoRuO_4H_4$' were annealed in evacuated silica tubes at 460 ºC. This resulted in the decomposition of the sample to form SrO, La_2O_3, Co, Ru and a number of other poorly crystalline phases, indicating the oxyhydride phase loses hydrogen under these conditions.

Running the $LaSr_3CoRuO_8$ + CaH_2 reactions for longer periods of time ($5 \times 7d$, compared to $3 \times 7d$ for sample C) does appear to enhance the asymmetry of SXRD reflections, suggesting the exsolution of SrO continues even after conversion of $LaSr_3CoRuO_8$ to $LaSrCoRuO_4H_4$, but given the difficulty in quantifying the concentration of $n > 1$ defect layers in samples it is hard to be definitive. Suffice to say that if it is possible to form $LaSrCoRuO_2H_4$ via this exsolution route it will require reaction times of many months.

We believe the exsolution of SrO from $LaSr_3CoRuO_4H_4$ is the first reported example of A-cation exsolution from a Ruddlesden-Popper phase, or indeed any perovskite-based oxide phase. The exsolution of B-site cations from ABO_3 transition-metal perovskite oxides under reducing conditions has been widely observed and studied because the exsolved metals form catalytically active nanoparticles which decorate the surfaces of the host materials.[38-42] Detailed studies have revealed that B-site exsolution and nanoparticle formation is favored by A-site deficiency of the host phase. Thus for example Ni is exsolved from $La_{0.52}Sr_{0.28}\square_{0.2}Ni_{0.06}Ti_{0.94}O_3$ (where $\square$ indicates a cation vacancy) but not $La_{0.3}Sr_{0.7}Ni_{0.06}Ti_{0.94}O_{3.09}$.[43] This behavior is rationalized by observing that the exsolution of B-cations from $A_{1-\delta}BO_3$ phases drives the sample stoichiometry towards the ideal ABO_3 formulation, and thus stability. The exsolution of SrO rather than Co or Ru from $LaSr_3CoRuO_4H_4$ is also consistent with this rationalization because the exsolution of B-cations would result in an A-cation rich A_2BO_4 phase for which there is no obvious mechanism to structurally accommodate the A-cation excess. In contrast exsolving A-cations yields a B-cation excess which can be simply accommodated by adding the $n > 1$ defect layers observed in the HAADF-STEM images of '$LaSr_3CoRuO_4H_4$'.

Magnetic characterization of '$LaSr_3CoRuO_4H_4$'. Magnetization data collected from sample B of '$LaSr_3CoRuO_4H_4$' indicate the presence of small quantities of elemental cobalt (< 1 wt%) in common with other cobalt-containing oxyhydride phases.[31, 44] We believe that the elemental Co was formed either by reduction of small quantities of Co_3O_4 left over from the synthesis of $LaSr_3CoRuO_4H_4$, or from sample decomposition, not from exsolution of the metal.

To measure the magnetic properties of the bulk '$LaSr_3CoRuO_4H_4$' in the presence of the ferromagnetic cobalt impurity, a ferrosubtraction measurement procedure was used, as described previously for $LaSr_3NiRuO_4H_4$ and detailed in the Supporting Information.[36] Figure 8 shows a plot of the paramagnetic susceptibility of '$LaSr_3CoRuO_4H_4$' as a function of temperature. These data can be fitted by the Curie-Weiss law in the range $25 < T / K < 300$, to yield a Curie constant of 1.058(3) cm^3 K mol^{-1} and a Weiss constant of -39.4(4) K, as shown in the inset to Figure 8. The measured Curie constant is close to the expected spin-only value for a combination of d^8, S = 1, Co^{1+} and d^6, S = 0, Ru^{2+} centers (C_{calc} = 1 cm^3 K mol^{-1}). On further cooling, the paramagnetic susceptibility exhibits a maximum at T ~ 10 K, and there is a sharp increase in the saturated ferromagnetic moment of the sample below 50 K. This combination

of features suggests the onset of magnetic order at low temperature. To investigate this, NPD data (WISH, ISIS) were collected from the sample at 2 K and are shown in Figure S6 in the Supporting Information. These data are identical to the analogous high-temperature data set, with
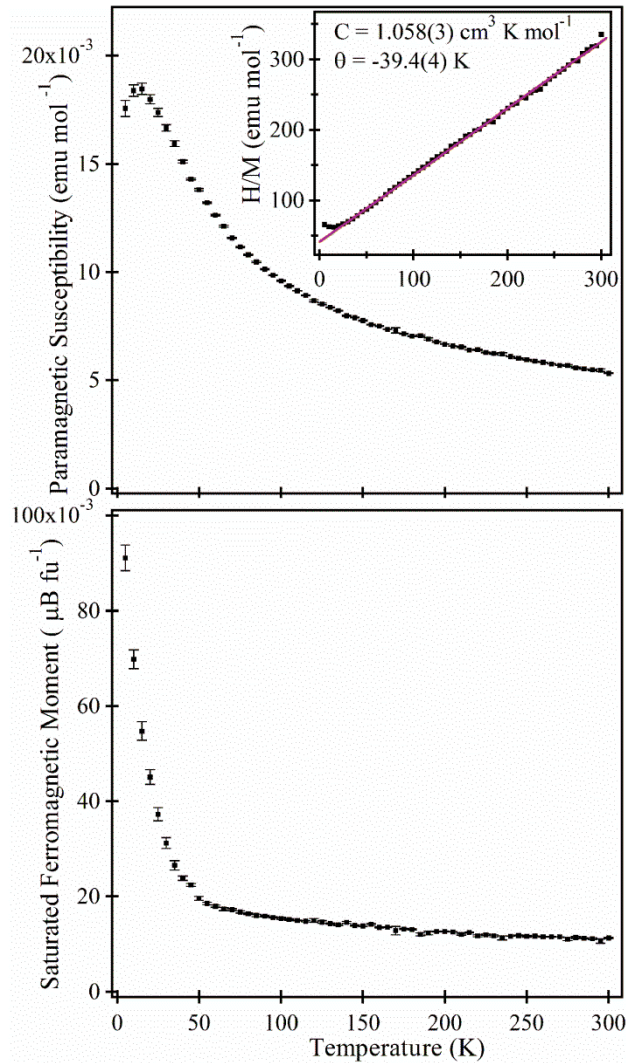

Figure 8. Paramagnetic susceptibility (top) and saturated ferromagnetic moment (bottom) of 'LaSr$_3$CoRuO$_4$H$_4$' (sample B) plotted as a function of temperature. Inset shows fit to the Curie-Weiss law in the range $25 < $ T// K $ < 300$.
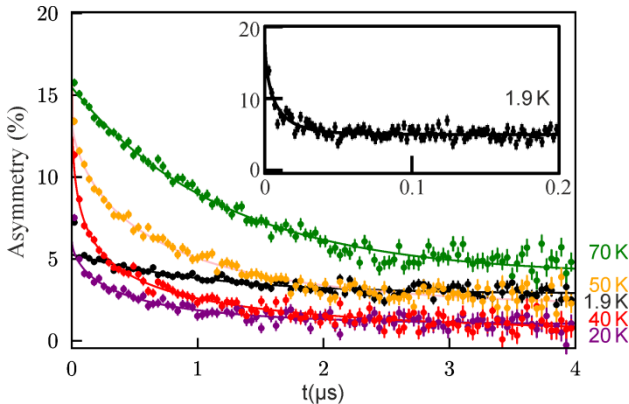

Figure 9. Plots of the asymmetry of μ$^+$SR data collected from sample C of LaSr$_3$CoRuO$_4$H$_4$ at various temperatures. Inset shows expansion of 1.9 K data set.

no indication of any magnetic scattering, thus providing no evidence for magnetic order in the phase at 2 K. μ$^+$SR data were also collected from sample C of 'LaSr$_3$CoRuO$_4$H$_4$' and plots of the asymmetry of the positron flux (Figure 9) show no evidence for magnetic order for T > 1.9 K. It should be noted that the data collected at 1.9 K are consistent with rapid relaxation of the muon spin polarization, suggesting the system is on the cusp of a magnetic ordering transition, however the lack of oscillations in the asymmetry data confirm there is no long-range magnetic order at this temperature. The lack of the long-ranger magnetic order in 'LaSr$_3$CoRuOH$_4$' is suprising given the $(d_{xz/yz})^4(d_{xy})^2(d_{x^2-y^2})^1(d_{z^2})^1$ eletronic configuration of Co^{1+} aligns a half-filled $d_{x^2-y^2}$ orbital with the 1s orbitals of the hydride anions. These orbtials will mix efficiently leading to the expectation of strong in-plane magnetic exchange interactions. The lack of long-range magnetic order, suggest that the diamagnetic Ru^{2+} centres in 'LaSr$_3$CoRuOH$_4$' block these in-plane exchange couplings in some way.

Conclusions

LaSr$_3$CoRuO$_8$ reacts with CaH$_2$ to first form LaSr$_3$CoRuO$_6$ and then the oxyhydride LaSr$_3$CoRuO$_4$H$_4$. However, in contrast to the analogous LaSr$_3$NiRuO$_8$/LaSr$_3$NiRuO$_4$H$_4$ nickel-based system, the formation of LaSr$_3$CoRuO$_4$H$_4$ is accompanied by the exsolution of SrO. The change in composition to the host phase is accommodated by the formation of $n > 1$ defect layers which accumulate in the Ruddlesden-Popper stacking sequence. This novel pseudo-topochemical process, if controlled, offers the prospect of forming $n > 1$ members of the La$_{n/2}$Sr$_{1+n/2}$Co$_{n/2}$Ru$_{n/2}$O$_{n+1}$H$_{2n}$ homologous series. If this processes can be applied to other Ruddlesden-Popper structured phases with sufficient control, it offers the opportunity to prepare metastable $n > 1$ Ruddlesden-Popper phases which cannot be synthesized by conventional high temperature routes.

Methods

Synthesis of LaSr$_3$CoRuO$_8$. Samples of LaSr$_3$CoRuO$_8$ were prepared by a high-temperature ceramic method. Suitable stoichiometric ratios of La$_2$O$_3$ (99.999%, dried at 900 °C), SrCO$_3$ (99.994%), RuO$_2$ (99.99%, dried at 800°C) and Co$_3$O$_4$ (99.9985%) were ground together using an agate mortar and pestle, transferred into an alumina crucible, and then heated at a rate of 1 °C min^{-1} to 1000 °C in air to decompose the carbonate. Samples were then reground, pressed into pellets and heated for 3 periods of 48 hours at 1200°C in air, with grinding between heating periods.

Anion-exchange reactions. A process similar to that used to convert LaSr$_3$NiRuO$_8$ into the oxide-hydride LaSr$_3$NiRuO$_4$H$_4$ [36] was used in an attempt to convert LaSr$_3$CoRuO$_8$ into LaSr$_3$CoRuO$_4$H$_4$. Samples of LaSr$_3$CoRuO$_8$ were ground together with approximately 4 mole equivalents of CaH$_2$ using an agate pestle and mortar in an argon filled glovebox. The resulting powders were sealed in silica ampoules and heated as described below, with the samples being reground between heating periods. Once the reactions were deemed complete, the reaction mixtures was washed, under nitrogen, with 8 × 25 ml of 0.1 M solution of NH$_4$Cl in methanol in order to remove the CaO formed as a by-product of the reaction, and any unreacted CaH$_2$. This was then followed by washing with 5 × 25 ml of clean methanol to dissolve NH$_4$Cl residues. The samples were

then dried under vacuum. Three samples were prepared: Sample A (0.3 g LaSr$_3$CoRuO$_8$) was heated for 7d periods between 350 ℃ and 460 ℃; Sample B (1.5 g LaSr$_3$CoRuO$_8$) heated for 3 periods of 7d at 460 ℃; Sample C (0.5 g LaSr$_3$CoRuO$_8$) heated for 7d at 450 ℃ then two periods of 7d at 460 ℃.

Characterization. Sample purity and reaction progress was monitored by X-ray powder diffraction (XRD) data collected from samples contained in gas-tight sample holders using a PANalytical X'Pert diffractometer incorporating an X'celerator position sensitive detector (monochromatic Cu Kα1 radiation). High-resolution synchrotron X-ray powder diffraction (SXRD) data were collected using instrument I11 at the Diamond Light Source Ltd. Diffraction patterns were collected using Si-calibrated X-rays with an approximate wavelength 0.825 Å, from samples sealed in 0.3 mm diameter borosilicate glass capillaries. Neutron powder diffraction (NPD) data were collected either using the WISH instrument (ISIS neutron source, UK) or the D2b instrument (ILL, France) from samples contained within vanadium cans. Rietveld profile refinements were performed using the GSAS suite of programs.[45] DC magnetization data were collected using a Quantum Design MPMS SQUID magnetometer. Thermogravimetric measurements were performed by heating powder samples at a rate of 5 ℃ min^{-1} under a flowing oxygen atmosphere, using a Mettler-Toledo MX1 thermogravimetric microbalance. Electron diffraction (ED) patterns were acquired on a FEI Tecnai transmission electron microscope operated at 200 kV. High angle annular dark field (HAADF) scanning transmission electron microscopy (STEM) images were acquired using a probe aberration corrected FEI Titan 80-300 "cubed" microscope operated at 300 kV. Samples for TEM analysis were prepared in the glove box filled with argon by grinding the material and dipping the copper TEM grid into the dry powder. A vacuum transfer holder was used to transfer the grids from the glove box to the microscope. Muon spin-resonance (μ$^+$SR) experiments were carried out at the Swiss Muon Source, PSI, Switzerland. In a μ$^+$SR experiment, spin-polarized muons were implanted in the bulk of a material and the time-dependence of their polarization monitored by recording the angular distribution of the subsequent positron decay.

ASSOCIATED CONTENT

Supporting Information. Structural characterization of LaSr$_3$CoRuO$_8$ by X-ray and neutron powder diffraction. Structural characterization of LaSr$_3$NiRuO$_4$H$_4$ by neutron powder diffraction. Further HAADF-STEM images of LaSr$_3$CoRuO$_4$H$_4$. Full description of FAULTS model. Description of 'Ferrosubtraction' method and 2 K neutron diffraction data set from LaSr$_3$CoRuO$_4$H$_4$. This material is available free of charge via the Internet at http://pubs.acs.org."

AUTHOR INFORMATION

Corresponding Author

* michael.hayward@chem.ox.ac.uk

Author Contributions

The manuscript was written through contributions of all authors.

ACKNOWLEDGMENT

REFERENCES

1. Hayward, M. A., Soft chemistry synthesis of oxides. In *Comprehensive Inorganic Chemistry II*, Reedijk, J.; Poeppelmeier, K. R., Eds. Elsevier: Oxford, 2013; Vol. 2, pp 417-453.

2. Schaak, R. E.; Mallouk, T. E., Perovskites by design: A toolbox of solid-state reactions. *Chem. Mater.* **2002,** *14*, 1455-1471.

3. Ranmohotti, K. G. S.; Josepha, E.; Choi, J.; Zhang, J. X.; Wiley, J. B., Topochemical Manipulation of Perovskites: Low-Temperature Reaction Strategies for Directing Structure and Properties. *Adv. Mater.* **2011,** *23*, 442-460.

4. Murphy, D. W.; Disalvo, F. J.; Carides, J. N.; Waszczak, J. V., Topochemical Reactions of Rutile Related Structures with Lithium. *Mater. Res. Bull.* **1978,** *13*, 1395-1402.

5. Cox, D. E.; Cava, R. J.; McWhan, D. B.; Murphy, D. W., A Neutron Powder Diffraction Study of the Lithium Insertion Compound LiMoO$_2$ from 4 - 440 K. *J. Phys. Chem. Solids* **1982,** *43*, 657-666.

6. Davidson, I. J.; Greedan, J. E., Neutron and X-Ray-Powder Diffraction Study of Li$_x$RuO$_2$ andLi$_x$IrO$_2$ - the Crystal-Structure of Li$_{0.9}$IrO$_2$. *J. Solid State Chem.* **1984,** *51*, 104-117.

7. Akimoto, J.; Gotoh, Y.; Oosawa, Y.; Nonose, N.; Kumagai, T.; Aoki, K.; Takei, H., Topotactic Oxidation of Ramsdellite-Type Li$_{0.5}$TiO$_2$, a New Polymorph of Titanium-Dioxide - TiO$_2$(R). *J. Solid State Chem.* **1994,** *113*, 27-36.

8. Latroche, M.; Brohan, L.; Marchand, R.; Tournoux, M., New Hollandite Oxides - TiO$_2$(H) and K$_{0.06}$TiO$_2$. *J. Solid State Chem.* **1989,** *81*, 78-82.

9. Watanabe, M.; Komatsu, Y.; Sasaki, T.; Fujiki, Y., A New Oxidation Process of Potassium Titanium-Dioxide Bronze with the Hollandite Structure. *J. Solid State Chem.* **1991,** *92*, 80-87.

10. Goodenough, J. B.; Kim, Y., Challenges for Rechargeable Li Batteries. *Chem. Mater.* **2010,** *22*, 587-603.

11. Etacheri, V.; Marom, R.; Elazari, R.; Salitra, G.; Aurbach, D., Challenges in the development of advanced Li-ion batteries: a review. *Energy & Environmental Science* **2011,** *4*, 3243-3262.

12. Gopalakrishnan, J.; Bhat, V., A$_2$Ln$_2$Ti$_3$O$_{10}$ (A = K or Rb, Ln = La or Rare-Earth) - a New Series of Layered Perovskites Exhibiting Ion-Exchange. *Inorg. Chem.* **1987,** *26*, 4299-4301.

13. Gopalakrishnan, J.; Bhat, V.; Raveau, B., A^{I}LaNb$_2$O$_7$ - a New Series of Layered Perovskites Exhibiting Ion-Exchange and Intercalation Behavior. *Mater. Res. Bull.* **1987,** *22*, 413-417.

14. Cushing, B. L.; Falster, A. U.; Simmons, W. B.; Wiley, J. B., A multivalent ion exchange route to lamellar calcium cobalt oxides, Ca$_x$CoO$_2$ (x < 0.5). *Chem. Commun.* **1996,** 2635-2636.

15. Cushing, B. L.; Wiley, J. B., Topotactic routes to layered calcium cobalt oxides. *J. Solid State Chem.* **1998,** *141*, 385-391.

16. Denis Romero, F.; Burr, S. J.; McGrady, J. E.; Gianolio, D.; Cibin, G.; Hayward, M. A., SrFe$_{0.5}$Ru$_{0.5}$O$_2$: sqaure-planar Ru^{2+} in an extended oxide. *J. Am. Chem. Soc.* **2013,** *135*, 1838-1844.

17. Amano Patino, M.; Zeng, D.; Bower, R.; McGrady, J. E.; Hayward, M. A., Coupled electronic and magnetic phase transition in the infinite-layer phase LaSrNiRuO$_4$. *Inorg. Chem.* **2016,** *55*, 9012-9016.

18. Hayward, M. A.; Green, M. A.; Rosseinsky, M. J.; Sloan, J., Sodium hydride as a powerful reducing agent for topotactic oxide deintercalation: synthesis and characterisation of the nickel (I) oxide LaNiO$_2$. *J. Am. Chem. Soc.* **1999,** *121*, 8843-8854.

19. Hayward, M. A.; Rosseinsky, M. J., Synthesis of the infinite layer Ni(I) phase NdNiO$_{2+x}$ by low temperature reduction of NdNiO$_3$ with sodium hydride. *Solid State Sci.* **2003,** *5*, 839-850.

20. Dixon, E.; Hadermann, J.; Ramos, S.; Goodwin, A. L.; Hayward, M. A., Mn(I) in an extended oxide - the synthesis and

characterisation of La$_{1-x}$A$_x$MnO$_2$. *J. Am. Chem. Soc.* **2011,** *133*, 18397-18405.

21.   Page, J. E.; Morgan, H. W. T.; Zeng, D.; Manuel, P.; McGrady, J. E.; Hayward, M. A., Sr$_2$FeIrO$_4$: square-planar Ir(II) in an extended oxide. *Inorg. Chem.* **2018,** *57*, 13577-13585.

22.   Page, J. E.; Hayward, M. A., Structure and magnetism of (La/Sr)$_2$M$_{0.5}$Ir$^{V\ 0.5}$O$_4$ and topochemically reduced (La/Sr)$_2$M$_{0.5}$Ir$^{II\ 0.5}$O$_3$ (M = Fe, Co) complex oxides. *Inorg. Chem.* **2049,** *58*, 6336-6343.

23.   Tsujimoto, Y.; Tassel, C.; Hayashi, N.; Watanabe, T.; Kageyama, H.; Yoshimura, K.; Takano, M.; Ceretti, M.; Ritter, C.; Paulus, W., Infinite-layer iron oxide with a square-plannar coordination. *Nature* **2007,** *450*, 1062-1065.

24.   Tassel, C.; Seinberg, L.; Hayashi, N.; Ganesanpotti, S.; Ajiro, Y.; Kobayashi, Y.; Kageyama, H., Sr$_2$FeO$_3$ with Stacked Infinite Chains of FeO$_4$ Square Planes. *Inorg. Chem.* **2013,** *52*, 6096-6102.

25.   Tassel, C.; Watanabe, T.; Tsujimoto, Y.; Hayashi, N.; Kitada, A.; Sumida, Y.; Yamamoto, T.; Kageyama, H.; Takano, M.; Yoshimura, K., Stability of the infinite layer structure with iron square planar coordination. *J. Am. Chem. Soc.* **2008,** *130*, 3764-3765.

26.   Li, R. K.; Greaves, C., Double-Layered Ruthenate Sr$_3$Ru$_2$O$_7$F$_2$ Formed by Fluorine Insertion into Sr$_3$Ru$_2$O$_7$. *Phys. Rev. B* **2000,** *62*, 3811-3815.

27.   Luo, K.; Johnson, R. D.; Tran, T. T.; Halasyamani, P. S.; Radaelli, P. G.; Hayward, M. A., Ba$_2$YFeO$_{5.5}$: A Ferromagnetic Pyroelectric Phase Prepared by Topochemical Oxidation. *Chem. Mater.* **2013,** *25*, 1800-1808.

28.   Yao, H. C.; Yao, Y. F. Y., Ceria in Automtive ExhaustCatalysts .1 Oxygen Storage. . *Journal of Catalysis* **1984,** *86*, 254-265.

29.   Kageyama, H.; Hayashi, K.; Maeda, K.; Attfield, J. P.; Hiroi, Z.; Rondinelli, J. M.; Poeppelmeier, K. R., Expanding frontiers in materials chemistry and physics with multiple anions. *Nat. Commun.* **2018,** *9*, 772.

30.   Harada, J. K.; Charles, N.; Poeppelmeier, K. R.; Rondinelli, J. M., Heteroanionic Materials by Design: Progress Toward Targeted Properties. *Adv. Mater.* **2019,** *31*.

31.   Hayward, M. A.; Cussen, E. J.; Claridge, J. B.; Bieringer, M.; Rosseinsky, M. J.; Kiely, C. J.; Blundell, S. J.; Marshall, I. M.; Pratt, F. L., The hydride anion in an extended transition metal oxide array: LaSrCoO$_3$H$_{0.7}$. *Science* **2002,** *295*, 1882-1884.

32.   Denis Romero, F.; Leach, A.; Moller, J. S.; Foronda, F.; Blundell, S.; Hayward, M. A., Strontium vanadium oxide-hydrides: 'square-planar' two-electron phases. *Angew. Chem., Int. Ed.* **2014,** *53*, 7556-7559.

33.   Rebbah, H.; Desgardin, G.; Raveau, B., Atimos Oxides - Cationic Exchangers. *Mater. Res. Bull.* **1979,** *14*, 1125-1131.

34.   Rebbah, H.; Pannetier, J.; Raveau, B., Localization of Hydrogen in the Layer Oxide HTiNbO$_5$. *J. Solid State Chem.* **1982,** *41*, 57-62.

35.   Jin, L.; Hayward, M. A., Rhodium-containing oxide-hydrides: covalently stabilized mixed-anion solids. *Chem. Commun.* **2019,** *55*, 4861-4864.

36.   Jin, L.; Lane, M.; Zeng, D.; Kirschner, F. K. K.; Lang, F.; Manuel, P.; Blundell, S. J.; McGrady, J. E.; Hayward, M. A., LaSr$_3$NiRuO$_4$H$_4$: a 4d transition-metal oxide-hydride containing metal hydride sheets. *Angew. Chem., Int. Ed.* **2018,** *57*, 5025-5028.

37.   Casas-Cabanas, M.; Reynaud, M.; Rikarte, J.; Horbach, P.; Rodriguez-Carvajal, J., FAULTS: a program for refinement of structures with extended defects. *J. Appl. Crystallogr.* **2016,** *49*, 2259-2269.

38.   Nishihata, Y.; Mizuki, J.; Akao, T.; Tanaka, H.; Uenishi, M.; Kimura, M.; Okamoto, T.; Hamada, N., Self-regeneration of a Pd-perovskite catalyst for automotive emissions control. *Nature* **2002,** *418*, 164-167.

39.   Du, Z. H.; Zhao, H. L.; Yi, S.; Xia, Q.; Gong, Y.; Zhang, Y.; Cheng, X.; Li, Y.; Gu, L.; Swierczek, K., High-Performance Anode Material Sr$_2$FeMo$_{0.65}$Ni$_{0.35}$O$_6$-delta with In Situ Exsolved Nanoparticle Catalyst. *Acs Nano* **2016,** *10*, 8660-8669.

40.   Neagu, D.; Oh, T. S.; Miller, D. N.; Menard, H.; Bukhari, S. M.; Gamble, S. R.; Gorte, R. J.; Vohs, J. M.; Irvine, J. T. S., Nano-socketed nickel particles with enhanced coking resistance grown in situ by redox exsolution. *Nat. Commun.* **2015,** *6*.

41.   Sun, Y. F.; Zhang, Y. Q.; Chen, J.; Li, J. H.; Zhu, Y. T.; Zeng, Y. M.; Amirkhiz, B. S.; Li, J.; Hua, B.; Luo, J. L., New Opportunity for in Situ Exsolution of Metallic Nanoparticles on Perovskite Parent. *Nano Lett.* **2016,** *16*, 5303-5309.

42.   Zhu, Y. L.; Zhou, W.; Ran, R.; Chen, Y. B.; Shao, Z. P.; Liu, M. L., Promotion of Oxygen Reduction by Exsolved Silver Nanoparticles on a Perovskite Scaffold for Low-Temperature Solid Oxide Fuel Cells. *Nano Lett.* **2016,** *16*, 512-518.

43.   Neagu, D.; Tsekouras, G.; Miller, D. N.; Menard, H.; Irvine, J. T. S., In situ growth of nanoparticles through control of non-stoichiometry. *Nat. Chem.* **2013,** *5*, 916-923.

44.   Helps, R. M.; Rees, N. H.; Hayward, M. A., Sr$_3$Co$_2$O$_{4.33}$H$_{0.84}$ – An extended transition metal oxide-hydride. *Inorg. Chem.* **2010,** *49*, 11062-11068.

45.   Larson, A. C.; Von Dreele, R. B. *General Structure Analysis System*, Los Alamos National Laboratory Report LAUR 86-748: 2000.